Zemin Mekaniği ve Geoteknik Mühendisliği
18. Ulusal Konferansı

29-30 Eylül 2022
Erciyes Üniversitesi, Kayseri

DOI:10.5505/2022zmgm.SS-72

ŞiLE KUMU ÜZERİNDE YAPILAN DİNAMİK ÜÇ EKSENLİ TESTLERDE AŞIRI BOŞLUK SUYU BASINCI OLUŞUMU VE TAHMİNİ

PREDICTION OF EXCESS PORE PRESSURES GENERATED DURING DYNAMIC TRIAXIAL TESTS ON SILE SAND

Abdülhakim ZEYBEK[1]

ÖZET

Deprem kaynaklı sıvılaşma, toplumlar üzerinde önemli sosyal, ekonomik ve psikolojik etkileri olan yıkıcı bir doğa olayıdır. Karmaşık yapısı nedeniyle geoteknik deprem mühendisliğinin en tartışmalı konularından birisi olan sıvılaşma, aşırı boşluk suyu basıncının artması ve nihayetinde zemin tabakasının mukavemetini ve rijitliğini yitirmesine neden olmaktadır. Tekrarlı yükler altında zeminlerde oluşan boşluk suyu basıncının tahmini için farklı ampirik modeller geliştirilmiştir. Bu modellerin performansı, esas olarak zemin özellikleri ve deney koşulları ile ilişkili olan ampirik katsayılara bağlıdır. Bu çalışmada, bir dizi gerilme kontrollü drenajsız dinamik üç eksenli deneyler gerçekleştirilerek Şile AFS 55/60 kumunun aşırı boşluk basıncı davranışı araştırılmıştır. Gevşek, orta sıkı ve sıkı olarak hazırlanan silindirik üç eksenli numuneler doygun hale getirilmiştir. Doygun zemin numuneleri 100 kPa efektif çevre gerilmesi altında izotropik olarak konsolide edilmiş ve ardından 0.1 Hz frekanstaki üniform tekrarlı deviatör gerilmelere tabi tutulmuştur. Elde edilen deneysel sonuçlar, literatürde yaygın olarak kullanılan gerilme tabanlı aşırı boşluk basıncı modelleri ile karşılaştırılmış ve Şile kumu için model parametreleri belirlenmiştir.

Anahtar Kelimeler: *Deprem, Sıvılaşma, Aşırı boşluk basıncı oluşumu, Temiz kum*

ABSTRACT

Earthquake-induced liquefaction is one of the most destructive phenomena of nature, having a major social, economic, and psychological impact on modern societies. Despite significant advances, liquefaction remains a controversial subject due to its complex nature. Liquefaction of soils is directly related to the build-up of excess pore pressures, causing significant degradation of effective stress and stiffness. In geotechnical earthquake engineering, several empirical models have been developed for predicting the excess pore pressures generated in soils during cyclic loading. The model performance is essentially controlled by the variation of empirical coefficients which depend on soil properties and test conditions. In this study, a series of stress-controlled undrained dynamic triaxial tests were conducted to investigate the excess pore pressure behavior of Sile AFS 55/60 sand.

[1] Asist. Prof., Muş Alparslan University, a.zeybek@alparslan.edu.tr (Abdülhakim ZEYBEK)

Cylindrical triaxial specimens were prepared in loose to dense conditions. The specimens were saturated, isotropically consolidated to an effective confining pressure of 100 kPa, and subsequently tested up to liquefaction at different cyclic stress ratios with a loading frequency of 0.1 Hz. The experimental data were compared with the prediction of stress-based excess pore pressure models widely used in the state of practice, and model parameters were modified for Sile sand.
Keywords: *Earthquake, Liquefaction, Excess pore pressure generation, Clean sand*

1. INTRODUCTION

Historical records reveal that severe liquefaction-induced damage has recurrently occurred in many moderate to strong earthquake events. Despite its recurrent feature over the last 200 years, the 1964 Good Friday-Alaska and Niigata-Japan earthquakes were the very first events that attracted the attention of geotechnical engineers to the destructive power of the liquefaction causing significant slope failures, sand boils, bearing capacity failures, and settlement and tilting of structures (i.e., Bartlett and Youd, 1992; Hamada, 1992). Since the 1964 earthquakes, extensive research has been conducted to gain a fundamental understanding of the liquefaction phenomenon. Despite these efforts, liquefaction is still a controversial research topic in geotechnical earthquake engineering due to its complicated nature, and further laboratory studies will be useful to improve the current state of knowledge of liquefaction.

Liquefaction is caused by the generation of excess pore pressures during cyclic loading in undrained conditions. Pore pressures become nearly equal to initial total stress, and effective stress approaches zero, significantly reducing the shear strength and stiffness of soil. The condition in which excess pore pressures (u_e) equal to initial effective confining stress (σ_o') for the first time ($r_u = \frac{u_e}{\sigma_o'} = 1$) is defined as initial liquefaction (Seed and Lee, 1966). The large axial strains developed during undrained cyclic loading (i.e., a double amplitude axial strain of 5 %) are also attributed to the initiation of liquefaction (Ishihara, 1993). Structures built on liquefiable soil deposits may suffer significant deformations.

Over the years, a large number of field (i.e., SPT, CPT) and/or laboratory tests (i.e., dynamic triaxial tests) have been performed to understand the behavior of soils under cyclic loading and elucidate the fundamental mechanisms of liquefaction, producing several empirical models to predict the excess pore pressure generation in sandy soils with or without fines (i.e., Seed et al., 1975; Booker et al., 1976; Polito et al., 2008; Baziar et al., 2011). These models are widely used in design practice as they are easy to use, time-efficient, and cost-effective. Further details about these models and their formulation will be given in the subsequent sections.

In this study, a series of 16 stress-controlled dynamic triaxial experiments were conducted to examine the excess pore pressure behavior of clean AFS 55/60 Sile sand during undrained cyclic loading. The sand specimens were prepared in loose, medium-dense, and dense conditions, isotropically consolidated and then subjected to a range of loading amplitudes with a loading frequency of 0.1 Hz. The experimental excess pore pressure data obtained under stress-controlled tests were compared with the excess pore pressure models commonly used in design practice to examine their performance, and model parameters were modified for Sile sand.

2. EXCESS PORE PRESSURE MODELS

As the liquefaction of soils is directly related to the build-up of excess pore pressures under cyclic loading, an accurate assessment of excess pore pressure is of great importance. For this purpose, different prediction methods (stress, strain, and energy-based models) have been developed. Amongst these, stress-based models have gained popularity. With this method, the excess pore pressure ratios (r_u) are related to the cycle ratio ($\frac{N}{N_{liq}}$). The cycle ratio is defined by the ratio between the number of loading cycles (N) and the number of cycles needed to initiate liquefaction (N_{liq}). Table 1 presents the most popular empirical stress-based models widely used in practice for the assessment of excess pore pressures generated in sand specimens with or without fines. The performance of the corresponding models is essentially controlled by the variation of empirical coefficients which depend on soil properties and test conditions and are typically determined through stress-controlled undrained cyclic tests.

Seed et al. (1975) used the experimental data of Lee and Albaisa (1974) and developed an empirical model to predict the excess pore pressure ratio. This model was later simplified by Booker et al. (1976). These models involve an empirical parameter (α), which is usually determined through undrained cyclic laboratory tests. Polito et al. (2008) used the same model suggested by Seed et al. (1975) but offered different α parameters varying as a function of relative density (D_r), fines content (FC), and cyclic stress ratio (CSR). In recent years, some researchers have modified these models by adding new parameters and have used the updated models to predict the experimental excess pore pressure ratio (i.e., Baziar et al., 2011).

Table 1. Excess pore pressure generation models

No	Models	Equation	Coefficients
1	Seed et al. (1975)	$r_u = \left\{\frac{1}{2} + \frac{1}{\pi} \cdot sin^{-1}\left[2 \cdot \left(\frac{N}{N_{liq}}\right)^{1/\alpha} - 1\right]\right\}$	$0.6 \leq \alpha \leq 1$ $\alpha = 0.7\ (for\ clean\ sand)$
2	Booker et al. (1976)	$r_u = \left\{\frac{2}{\pi} \cdot sin^{-1}\left[\left(\frac{N}{N_{liq}}\right)^{1/2\cdot\alpha}\right]\right\}$	$0.6 \leq \alpha \leq 1$ $\alpha = 0.7\ (for\ clean\ sand)$
3	Polito et al. (2008)	$r_u = \left\{\frac{1}{2} + \frac{1}{\pi} \cdot sin^{-1}\left[2 \cdot \left(\frac{N}{N_{liq}}\right)^{1/\alpha} - 1\right]\right\}$	$\alpha = 0.01166 \cdot FC + 0.007397 \cdot D_r + 0.01034 \cdot CSR + 0.5058$
4	Baziar et al. (2011)	$r_u = \left\{\frac{2}{\pi} \cdot sin^{-1}\left[\left(\frac{N}{N_{liq}}\right)^{1/2\cdot\alpha}\right]\right\} + \beta\sqrt{1 - \left\{\frac{2 \cdot N}{N_{liq}} - 1\right\}^2}$	$0.6 \leq \alpha \leq 0.8$ $0.0 \leq \beta \leq 0.25$
5	Khashila et al. (2017)	$r_u = 0.9 \cdot \left(\frac{N}{N_{liq}}\right)^r$	$r = 0.32 - 0.63$

3. EXPERIMENTAL STUDY

In this study, a total of 16 stress-controlled dynamic triaxial tests were performed in undrained conditions. The triaxial specimens were prepared in loose ($D_r = 38 - 43\%$), medium-dense ($D_r = 59 - 64\%$), and dense ($D_r = 84 - 89\%$) conditions. A summary of the experimental program and typical test results are given in Table 2.

Table 2. Typical test parameters and test results

Test No	Test ID	D_r (%)	u_0 (kPa)	σ_c' (kPa)	Frequency (Hz)	CSR	N_{liq}
1	AZ1		350	100	0.1	0.11	49
2	AZ2		350	100	0.1	0.12	33
3	AZ3	38-43	350	100	0.1	0.13	23
4	AZ4		350	100	0.1	0.15	11
5	AZ5		350	100	0.1	0.20	5
6	AZ6		350	100	0.1	0.18	155
7	AZ7		350	100	0.1	0.20	44
8	AZ8	59-64	350	100	0.1	0.21	24
9	AZ9		350	100	0.1	0.23	7
10	AZ10		350	100	0.1	0.25	2
11	AZ11		350	100	0.1	0.20	308
12	AZ12		350	100	0.1	0.22	90
13	AZ13	84-89	350	100	0.1	0.23	51
14	AZ14		350	100	0.1	0.25	18
15	AZ15		350	100	0.1	0.27	8
16	AZ16		350	100	0.1	0.30	4

2.1. Test Material

The test material used in this study was clean silica sand (AFS 55/60), obtained from a sand quarry in the Sile region of Istanbul. The physical properties of the sand were determined following the procedures described in ASTM standards. Figure 1 presents the result of the dry sieve analysis and its comparison with some of the standard sands widely used in the literature and liquefaction boundaries defined by Tsuchida (1970).

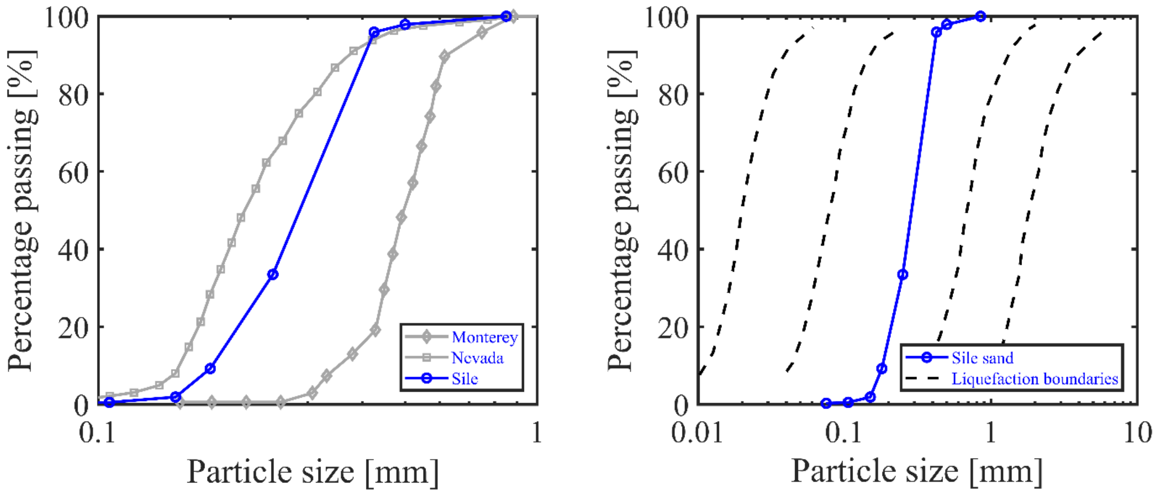

Figure 1. Particle size distribution of Sile sand

The average particle size (D_{50}) was 0.296, and the uniformity coefficient (C_u) was 1.352. It was classified as poorly graded sand according to the United Soil Classification System (USCS). Following Method 1A in D4253-16e1 (ASTM, 2019) and Method A in D4254-16 (ASTM, 2016), the minimum and maximum void ratios of Sile sand were found to be 0.574 and 0.885, respectively. As per the D854-14 (ASTM, 2014), the specific gravity (G_s) of Sile sand was determined as 2.65.

2.2. Testing Apparatus

Figure 2 shows the main component of the Dynatriax EmS system used during the stress-controlled dynamic triaxial experiments. It is a fully automated test system, manufactured by Wykeham Farrance - Controls Groups.

This type of test system consists of a triaxial reaction frame, a triaxial cell, a compact dynamic controller, a drive, an electromechanical actuator with 15 kN dynamic load capacity, an automatic volume change device, two air/water cylinders, an air receiver, a valve panel, a water distribution panel that controls water flow, an air compressor, a de-airing tank, and a vacuum pump. The cell, back, or excess pore pressures and axial load/displacements can be directly measured through the load cells and displacement or pressure transducers. The software and data acquisition system allow automatic control of excess pore pressure dissipation after liquefaction through the solenoid valve for the drainage line. The Dynatriax software and dynamic data acquisition system enable automatic control of the test stages including saturation, isotropic consolidation, and cyclic loading. The dynamic actuator of the test system can apply loading cycles (i.e., sinusoidal) in the range of 0.01-10 Hz, and the tests can be conducted in accordance with the D5311/D5311M-13 (ASTM, 2013).

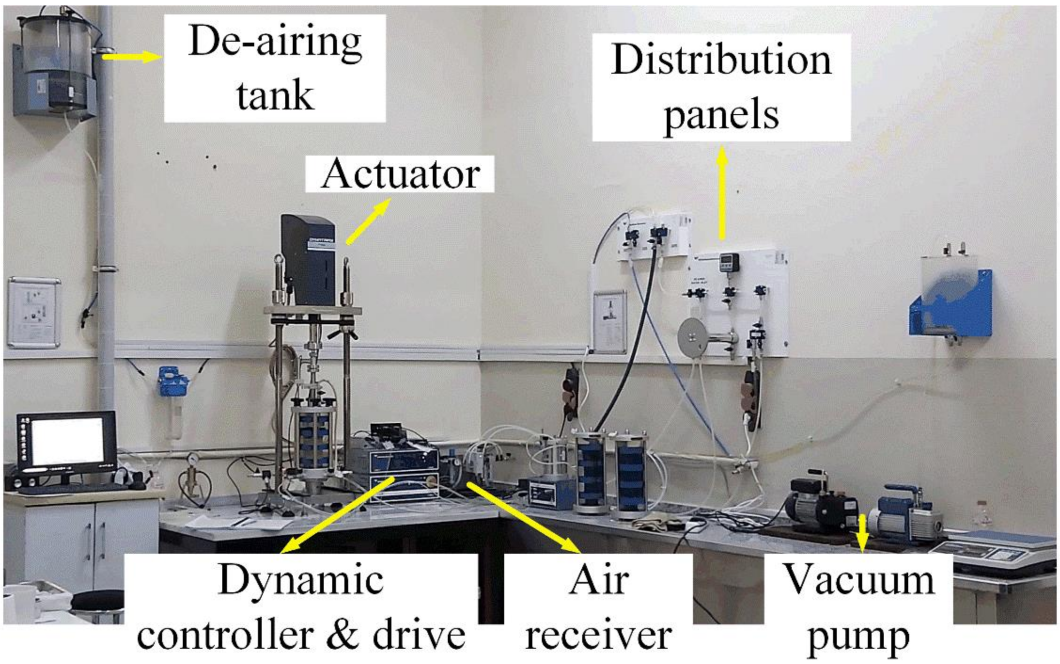

Figure 2. A view of the dynamic triaxial test system located in the Civil Engineering Laboratory of Mus Alparlsan University

2.3. Sample Preparation and Testing Procedure

The drainage lines were flushed with de-aired water, a priori. A porous stone and filter paper were placed on the base pedestal of the triaxial cell. A rubber-latex membrane was attached to the base pedestal and secured with two O-rings. A cylindrical split mold with a height of 140 mm and diameter of 70 mm was placed in its position, and the membrane was folded over this rigid mold. Vacuum pressure was supplied to ensure that membrane was stretched tight. The sand was dried in the oven, and the dried-oven sand was used to prepare samples inside the mold.

The oven-dried sand was dry pluviated into the mold from a constant height to prepare specimens in loose to medium dense conditions. The outlet of the funnel was altered by using different two diameters of acrylic tubes, which controlled the rate of sand flow and therefore the density of specimens. The dense specimens were prepared using the dry tamping method. In this method, dry sand was compacted in 10 equal layers by freely dropping a tamper from a predetermined height (typically 20 mm) and applying a standard number of blows (typically 25) in each layer.

After specimen preparation at the desired density, the top surface of each specimen was carefully leveled, and porous stone, filter paper, and the vacuum top cap were placed. The membrane was slipped to the top cap, and secured with a pair of O-rings. Vacuum pressure (-20 kPa) was applied to the specimens to ensure that they remained vertical and held themselves after the split mold was taken apart. The height of the specimens was measured following the removal of the split mold, and cylindrical triaxial specimens with a diameter of 70 mm and a height/diameter ratio of approximately 2 were obtained. The vacuum pressure was released after 20 kPa cell pressure was applied to the specimens which were set in the triaxial cell. Figure 3 displays typical images recorded at different stages of specimen preparation.

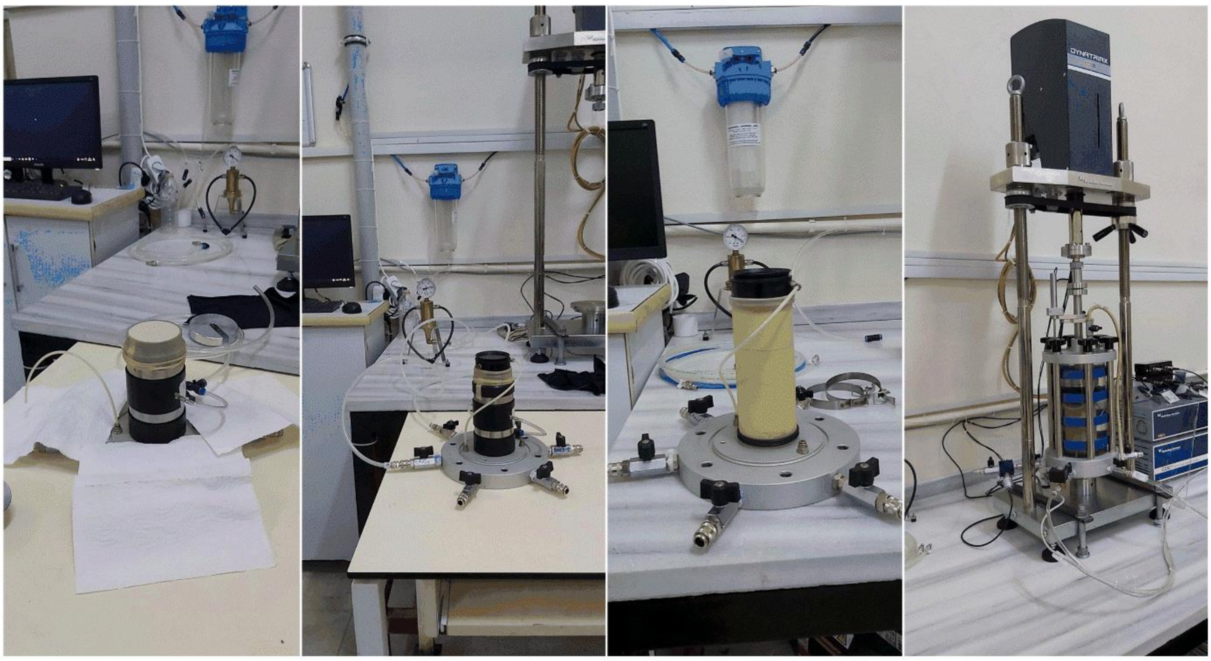

Figure 3. Preparation of triaxial specimens

The specimens were flushed with carbon dioxide gas and then de-aired water. This was followed by the application of back pressure to saturate the specimens. The cell and back pressure was gradually increased with a constant differential pressure of 10 kPa. The Skempton's pore pressure coefficient B was periodically measured to check the status of saturation. Before the consolidation stage, Skempton's B value was over 0.97 in each test. The saturated specimens were isotropically consolidated to effective stress of 100 kPa, and then subjected to cyclic loading with a frequency of 0.1 Hz and cyclic stress ratios in the range of 0.11 to 0.3. The specimens were tested until the excess pore pressure ratio (r_u) approached 1.

4. RESULTS AND DISCUSSION

Figure 4 shows typical dynamic triaxial test data recorded for a loose sand specimen subjected to a cyclic stress ratio of 0.2. The variation of excess pore pressure (u_e) or excess pore pressure ratio (r_u) with the number of loading cycles (N) are presented along with the effective stress path in q-p' plane.

It is seen that excess pore pressures developed under undrained cyclic loading and reached initial effective confining stress at the end of about 5 loading cycles. The excess pore pressure of 100% ($r_u = 1$) corresponded to the onset of liquefaction. The rate of excess pore pressure rise was accelerated beyond ($r_u = 0.7 - 0.75$). The specimen after this point was observed to start suffering large axial strains. The build-up of excess pore pressure led to a significant reduction in the mean effective stress (p') and stress path moved towards the critical state.

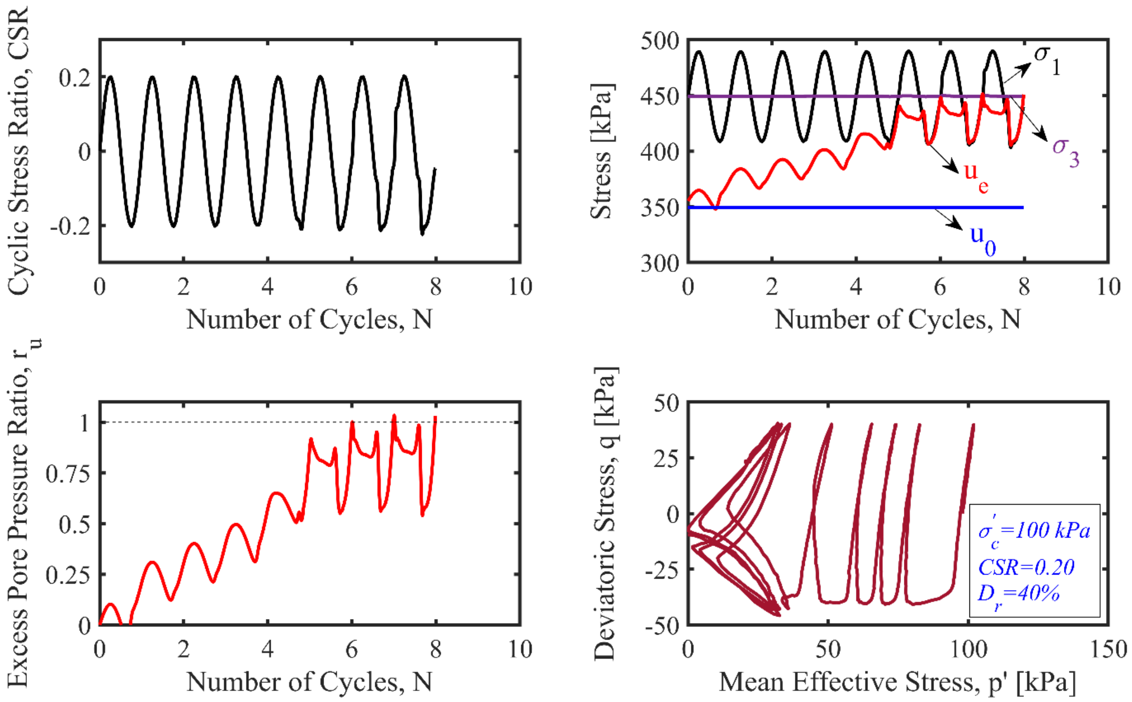

Figure 4. Typical cyclic behavior of sand

In the current study, the tests were conducted at the same effective confining stress and three different relative densities. Figure 5 plots the relationship between the cyclic stress ratio (CSR) and the number of cycles required for liquefaction (N_{liq}) to show the general trend followed by the experimental data collected in this work. It appears that at the same density N_{liq} reduced as the specimens were tested under larger deviatoric stresses. At the same N_{liq}, the denser specimens required much larger deviatoric stress. These results show that relative density is one of the most important parameters significantly affecting the liquefaction resistance of the sand, and excess pore pressure models should take this into account.

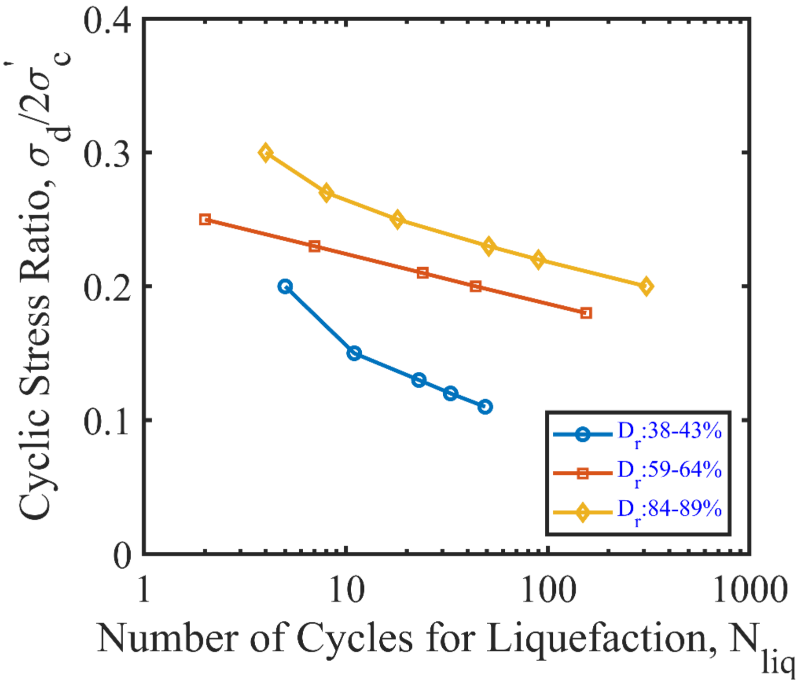

Figure 5. Relationship between cyclic stress ratio and number of cycles required for liquefaction

Based on the upper and lower bounds experimentally determined by Lee and Albaisa (1974), α parameter was suggested to be taken as 0.7 for clean sand (Seed et al., 1975; Booker et al., 1976). Baziar et al. (2011) modified Booker's method by adding another constant β which is a function of silt content. Polito et al. (2008) proposed an empirical correlation for calculating α parameter as a function of fines content, relative density, and cyclic stress ratio. For sands with low fines content ($FC < 35\%$), this parameter was shown to be relatively independent of the cyclic stress ratio. This indicates that α parameter for clean sand is mainly governed by the change in relative density.

Figure 6 compares the predictions of such models with the excess pore pressure data obtained through stress-controlled tests conducted on specimens of clean sand. For this analysis, excess pore pressure ratios (r_u) measured at different relative densities and cyclic stress ratios are plotted against normalized cycle ratios ($\frac{N}{N_{liq}}$). It is seen that using the α values proposed by Seed et al. (1975) and Polito et al. (2008), most of the test data particularly at the early stages of cyclic loading appear to deviate from the predicted boundaries, underestimating the build-up of excess pore pressures. The method of Baziar et al. (2011) seems to provide a reasonable prediction of excess pore pressures, engulfing the majority of the experimental data.

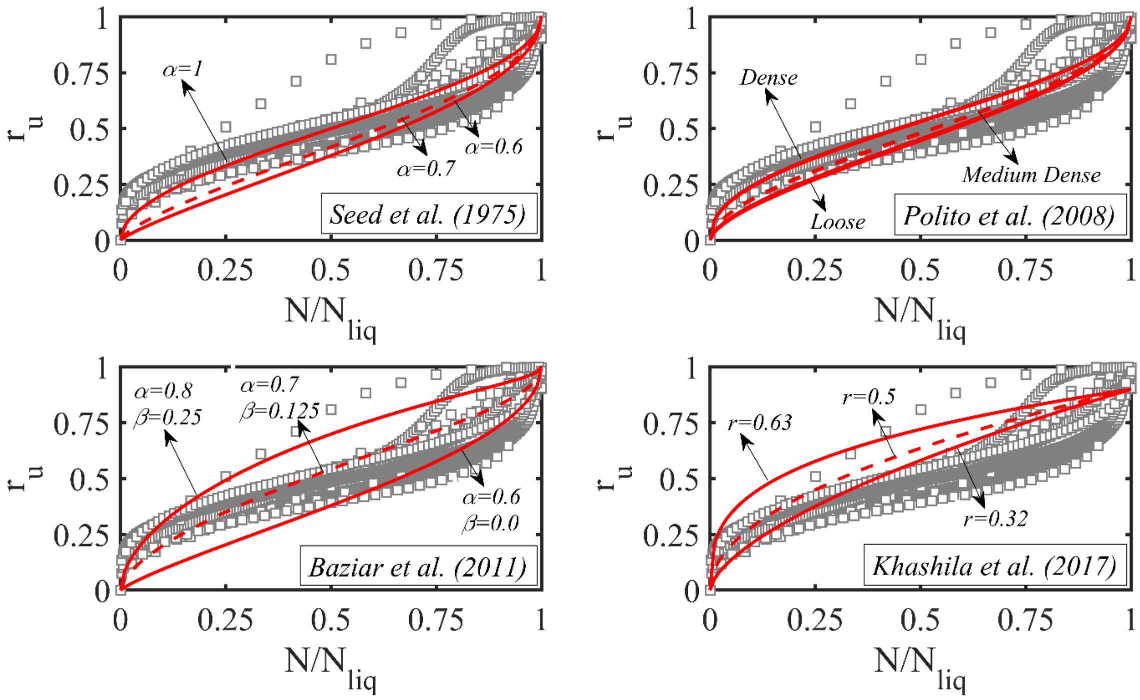

Figure 6. Comparison of experimental data with the predictions of excess pore pressure models

The above-mentioned results suggest that the performance of the excess pore pressure models strongly relies on the empirical parameter α and reveal the need for using an updated α parameter. With this aim, new α values and boundaries were determined through a simple statistical analysis conducted on the test data. It is evident from Figure 7 that using the updated α parameters. Seed's method can successfully capture most of the experimental data points.

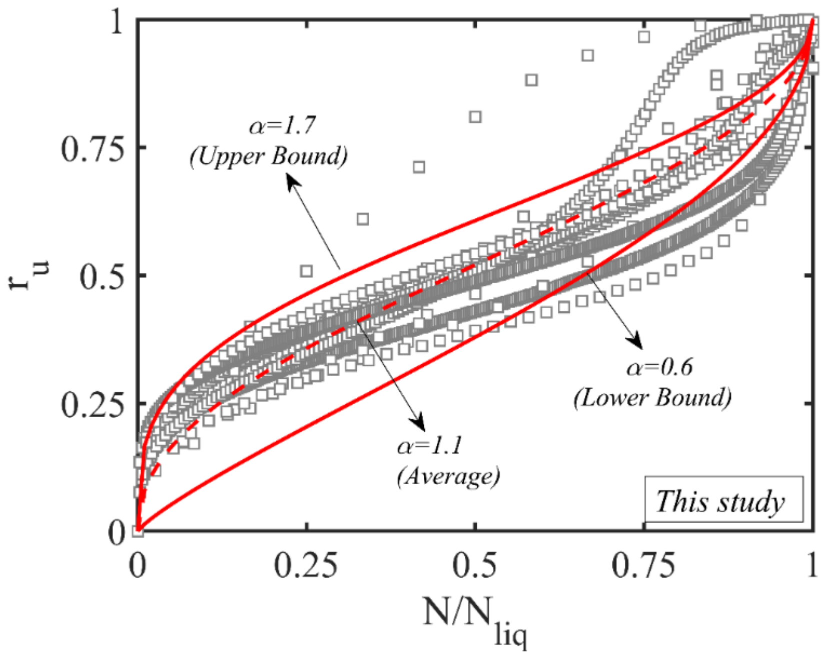

Figure 7. The effect of α parameter on the empirical prediction of the excess pore pressure

It is worth noting that none of the empirical models discussed above was capable of adequately capturing the excess pore pressure generation recorded at high cyclic stress ratios where liquefaction was reached after a few loading cycles only. The measured excess pore pressure data was underestimated by most of the models. The closest match was obtained using the approach proposed by Khashila et al. (2017) and using the fitting constant α=0.63.

5. CONCLUSIONS

The generation of excess pore pressure during cyclic loading and its prediction is one of the important research topics in the field of geotechnical earthquake engineering. Several empirical models have been developed for the estimation of excess pore pressures generated in sandy soils with or without fines, and the accuracy of the model predictions relies on the fitting parameters which are a function of soil characteristics, test, and loading conditions. This study presents the results of 16 dynamic triaxial tests conducted on reconstituted sand specimens prepared in loose, medium-dense, and dense conditions. The measured excess pore pressures were compared with the predictions of several stress-based excess pore pressure models widely used in design practice. The following conclusions were made from this study:

1. In all cases, excess pore pressures were generated and approached the initial effective confining stress, causing significant degradation of stiffness of clean sand specimens. The number of cycles required for liquefaction was a function of the level of applied cyclic stress and density of specimens. Regardless of the relative density, the specimens liquefied at lower loading cycles when subjected to higher cyclic stress ratios.

2. As the relative density and cyclic stress ratio significantly affect the excess pore pressure behavior of sandy soils, the incorporation of these parameters is of great importance for the accurate estimation of excess pore pressures.

3. The model proposed by Baziar et al. (2011) provided reasonably better predictions than the other three models, engulfing the majority of the measured excess pore pressure data. The estimations of other models such as that of Seed et al. (1975) were improved by updating the model parameters.

4. For the range of cyclic stress ratios (0.11 to 0.3) and relative densities (38 to 89%) tested in the current study, the constant α that provided the best fit to the experimental data was found to be 0.6 (lower bound), 1.1 (average), and 1.7 (upper bound) for clean Sile sand. Further tests at different levels of fines content, cyclic stress ratio, and density are expected to provide more accurate fitting constants for this type of sand and will help to better calibrate the model parameters.

ACKNOWLEDGMENT

The author would like to thank Murat ULU and Tahsin CALP for their technical aid during the experimental work.

REFERENCES

ASTM International (2013), "Standard Test Method for Load Controlled Cyclic Triaxial Strength of Soil", D5311/D5311M-13, West Conshohocken, PA: ASTM International, updated November 1, 2013. https://doi.org/10.1520/D5311_D5311M-13

ASTM International (2014), "Standard Test Methods for Specific Gravity of Soil Solids by Water Pycnometer", D854-14, West Conshohocken, PA: ASTM International, updated May 1, 2014. https://doi.org/10.1520/D0854-14

ASTM International (2016), "Standard Test Methods for Minimum Index Density and Unit Weight of Soils and Calculation of Relative Density", D4254-16, West Conshohocken, PA: ASTM International, updated March 1, 2016. https://doi.org/10.1520/D4254-16

ASTM International (2019), "Standard Test Methods for Maximum Index Density and Unit Weight of Soils Using a Vibratory Table", D4253-16e1, West Conshohocken, PA: ASTM International, updated November 22, 2019. https://doi.org/10.1520/D4253-16E01

Bartlett, S.F., Youd, T.L. (1992), "Case Histories of Lateral Spreads Caused by the 1964 Alaska Earthquake, Case Studies of Liquefaction and Lifeline Performance during Past Earthquakes", Vol 2, Technical Report, NCEER-92-0001, NCEER, Buffalo, NY, Hamada, M., and T.D. O'Rourke (eds): 2.1-2.125. Available at: https://www.buffalo.edu/mceer/catalog.host.html/content/shared/www/mceer/publications/NCEER-92-0002.detail.html

Baziar M.H., Shahnazari, H., Sharafi, H. (2011), "A Laboratory Study on the Pore Pressure Generation Model For Firouzkooh Silty Sands Using Hollow Torsional Test", International Journal of Civil Engineering, Vol 9, 2, 126-134. Available at: http://ijce.iust.ac.ir/article-1-489-en.html

Booker, J.R., Rahman, M.S., Seed, H.B. (1976), "A Computer Program for the Analysis of Pore Pressure Generation and Dissipation during Cyclic or Earthquake Loading", Berkeley, Earthquake Engineering Center, University of California. Available at: https://nehrpsearch.nist.gov/static/files/NSF/PB263947.pdf

Hamada, M. (1992), "Large Ground Deformations and Their Effects on Lifeline: 1964 Niigata Earthquake, Case Studies of Liquefaction and Lifeline Performance during Past Earthquakes", Vol 1, Technical Report, NCEER-92-0001, NCEER, Buffalo, NY, Hamada, M., and T.D. O'Rourke (eds): 3.1-1.99.

Ishihara, K. (1993), "Liquefaction and Flow Failure During Earthquakes", Géotechnique, Vol 43, 3, 351-451. https://doi.org/10.1680/geot.1993.43.3.351

Khashila, M., Hussien, M.N., Karray, M., Chekired, M. (2017), "Use of Pore Pressure Build-Up as Damage Metric in Computation of Equivalent Number of Uniform Strain Cycles", *Canadian Geotechnical Journal*, Vol 55, 4, 538-550. https://doi.org/10.1139/cgj-2017-0231

Lee, K.L., Albaisa, A. (1974), "Earthquake Induced Settlements in Saturated Sands", Journal of the Soil Mechanics and Foundations Division, Vol 100, 4. https://doi.org/10.1061/AJGEB6.0000034

Polito, C.P., Green, R.A., Lee, J. (2008), "Pore Pressure Generation Models for Sands and Silty Soils Subjected to Cyclic Loading", Journal of Geotechnical and Geoenvironmental Engineering, Vol 134, 10, 1490-1500. https://doi.org/10.1061/(ASCE)1090-0241(2008)134:10(1490)

Seed, H.B. Lee, K. L. (1966), “Liquefaction of Saturated Sands during Cyclic Loading”, Journal of the Soil Mechanics and Foundations Division, Vol 92, 6, 105-134. https://doi.org/10.1061/JSFEAQ.0000913

Seed, H.B., Idriss, I.M., Makdisi, F., Banerjee, N. (1975), “Representation of Irregular Stress Time Histories by Equivalent Uniform Stress Series in Liquefaction Analyses”, EERC 75-29. Earthquake Engineering Research Center, University of California, Berkeley.

Tsuchida, H. (1970), “Prediction and Countermeasure Against Liquefaction the Liquefaction in Sand Deposits”, Paper presented at the Seminar, Port and Harbour Research Institute, Ministry of Transport.

SYMBOLS

B	**Skempton's Pore Pressure Coefficient**	**CSR**	**Cyclic Stress Ratio**
D_r	**Relative Density**	**FC**	**Fines Content**
N	**Number of Loading Cycles**	N_{liq}	**Number of Cyles to Liquefaction**
r_u	**Excess Pore Pressure Ratio**	u_e	**Excess Pore Pressure**
u_0	**Back Pressure**	α	**Empirical Fitting Constant**
σ'_c	**Effective Confining Stress**	σ_d	**Deviatoric Stress**
σ'_o	**Initial Effective Confining Stress**	u_e	**Excess Pore Pressure**